Elucidation of the Paramagnetic R_1 Relaxation of Heteronuclei and Protons in Cu(II) Plastocyanin from *Anabaena variabilis*

Lixin Ma,[†] Anne-Marie M. Jørgensen,[†] G. Ole Sørensen,[†] Jens Ulstrup,[‡] and Jens J. Led*[,†]

Contribution from the Department of Chemistry, University of Copenhagen, The H. C. Ørsted Institute, Universitetsparken 5, DK-2100 Copenhagen Ø, Denmark, and the Department of Chemistry, The Technical University of Denmark, Building 207, DK-2800 Lyngby, Denmark

Received April 19, 2000. Revised Manuscript Received July 19, 2000

Abstract: The longitudinal paramagnetic dipolar relaxation rates, R_{1p}, of ^{15}N, ^{13}C, and ^{1}H nuclei in plastocyanin from *Anabaena variabilis* (*A.v.* PCu) were determined at 11.7 and 17.6 T from the corresponding experimental relaxation rates in reduced (R_{1d}) and partly oxidized (R_{1o}) *A.v.* PCu. To obtain an accuracy of the relaxation data sufficiently high for the subsequent analysis, the experimental rates were determined by a simultaneous least-squares analysis of all the spectra in a relaxation experiment. Also, a refined solution structure of *A.v.* PCu was determined from 1459 NOE distance restraints and 87 angle restraints by distance geometry, simulating annealing and restrained energy minimization. The average rms deviation from the mean structure of the 20 structures with the lowest total energy is 0.75 Å for the backbone atoms and 1.21 Å for all heavy atoms. The distance information of the dipolar paramagnetic R_{1p} rates was compared with the corresponding distances in the refined NMR solution structure. The comparison reveals that the point dipolar approximation, which assumes that R_{1p} is caused by a dipolar interaction of the nuclei with the *metal*-centered unpaired electron of the Cu^{2+} ion, does not apply to the heteronuclei. In the case of protons it applies only for proton−copper distances shorter than ∼10 Å. In contrast, it is found that the R_{1p} relaxation of the ^{15}N and ^{13}C nuclei is dominated by dipolar interaction with unpaired metal electron spin density delocalized onto the $2p_z$ orbitals of the heteronuclei. From the R_{1p} rates of the heteronuclei and the metal−nuclei distances in the refined NMR solution structure, the delocalized unpaired spin densities ρ^{π} of the individual ^{15}N and ^{13}C nuclei were derived. It is found that ρ^{π} decays approximately exponentially with the metal−nuclei distance and almost isotropically throughout the protein. Possible implications of this decay for the electron-transfer pathways of *A.v.* PCu are discussed.

Introduction

Nuclear paramagnetic relaxation is a potential source of information about the structure and function of metalloproteins directly in their natural aqueous media. Thus, it holds information about the electron relaxation and, thereby, about the geometry of the metal site. Furthermore it can give information about electron-transfer rates, electron density delocalization, and electron spin polarization and may, in this way, provide valuable information about possible electron-transfer pathways. In principle, it can also yield long-range geometric distance information that reaches beyond the upper limit of ∼5 Å obtainable from $^{1}H-^{1}H$ dipolar interactions in NOE spectra of diamagnetic proteins. Nuclear paramagnetic relaxation may, therefore, provide complementary long-range distance information valuable in NMR determination of protein solution structures.

However, nuclear paramagnetic relaxation is a complicated function of electron−nuclear distances, molecular dynamics, electron relaxation, electron−nucleus couplings, and rates of possible exchange processes, e.g., the electron-transfer rates. Moreover, precise determination of the nuclear relaxation rates can be hampered by excessive line widths and signal overlap caused by unfavorable electron relaxation rates. Determination of nuclear paramagnetic relaxation rates is, therefore, difficult unless conditions that simplify the nuclear paramagnetic relaxation can be applied and a sufficiently versatile set of experimental data can be obtained.

In addition to these experimental complications, a precise interpretation of the nuclear paramagnetic relaxation caused by the electron−nuclear dipolar interaction can be difficult for two reasons. First, both *metal*-centered and *ligand*-centered unpaired electron spin density can contribute to the nuclear relaxation[1,2] which, in turn, can prevent an accurate and reliable determination of electron spin delocalization and electron−nuclear distances from the paramagnetic nuclear relaxation in proteins. Theoretical considerations suggest[2] that this holds in particular for paramagnetic relaxation of heteronuclei such as ^{13}C and ^{15}N. Second, the size of the electron relaxation time and its contribution to the effective correlation time for the electron−nuclear interaction are not always known with sufficient accuracy.

Plastocyanin from *Anabaena variablis* (*A.v.* PCu) is a small blue copper protein (105 amino acids, M_r 10.5 kDa) which functions as an electron carrier in the electron-transfer process of photosynthesis. The fast electron self-exchange rate of this protein makes it suitable for studies of the paramagnetic relaxation enhancement caused by the unpaired electron of the Cu^{2+} ion. Thus, the fast electron self-exchange between reduced and oxidized *A.v.* PCu in mixtures of the two species provides an excellent system for observing the Cu^{2+}-induced paramag-

* To whom correspondence should be addressed: (telephone) (+45) 3532 0302; (fax) (+45) 3535 0609; (e-mail) led@kiku.dk.
[†] University of Copenhagen.
[‡] The Technical University of Denmark.

(1) Solomon, I. *Phys. Rev.* **1955**, *99*, 559−565.
(2) Gottlieb, H. P. W.; Barfield, M.; Doddrell, D. M. *J. Chem. Phys.* **1977**, *67*, 3785−3794.

10.1021/ja001368z CCC: $19.00
Published on Web 09/13/2000

netic enhancement of the relaxation of the nuclei in the reduced form. Furthermore, the relaxation time of the unpaired electron of the Cu^{2+} ion in *A.v.* PCu was recently determined with high accuracy,[3] allowing a reliable estimation of the effective correlation time for the electron−nuclear interaction.

Here we present a detailed analysis of the paramagnetic longitudinal relaxation of ^{15}N, ^{13}C, and ^{1}H nuclei in oxidized *A.v.* PCu using a mixed system of the reduced and oxidized forms of the protein. The analysis is based upon accurate determination of the size of the paramagnetic longitudinal relaxation rates R_{1p} of the nuclei in the protein and a refined NMR solution structure also determined here. The combined knowledge of the solution structure and the R_{1p} rates of the protein allows an unraveling of the dipolar nuclear−electron interaction, clarifies the possibilities of obtaining intramolecular distances from nuclear paramagnetic relaxation enhancement, and yields information about delocalization of the unpaired metal electron and spin polarization in the protein. It also provides insight into the possibility of obtaining information about electron-transfer pathways in blue copper proteins from the paramagnetic relaxation enhancement of the nuclei of the proteins.

Theoretical Section

Longitudinal Paramagnetic Relaxation of Ligand Nuclei. The longitudinal relaxation of the ligand nuclei in paramagnetic metal complexes is affected by the unpaired electrons via three different mechanisms:

$$R_{1p} = R_{1dip} + R_{1cont} + R_{1Curie} \tag{1}$$

where R_{1p} is the total paramagnetic relaxation rate. In eq 1, the dipolar relaxation rate, R_{1dip}, is caused by modulation of the dipolar interaction between the nuclear spin I and the total electron spin S ($^1/_2$ for Cu(II) proteins). For $I = {}^1/_2$ it is given by[1,2]

$$R_{1dip} = \frac{2}{15}\left(\frac{\mu_0}{4\pi}\right)^2 S(S+1) g_e^2 \mu_B^2 \gamma_I^2 \Delta^2 \left[\frac{3\tau_{c,1}}{1+\omega_I^2\tau_{c,1}^2} + \frac{7\tau_{c,2}}{1+\omega_S^2\tau_{c,2}^2}\right] \tag{2}$$

In Solomon's original formalism $\Delta = r_M^{-3}$, where r_M is the distance between the nucleus and the unpaired electrons located at the metal ion. The correlation rates $\tau_{c,k}^{-1}$ ($k = 1, 2$) that characterize the modulation of the interaction are given by $\tau_{c,k}^{-1} = \tau_R^{-1} + R_{ke} + \tau_j^{-1}$, where τ_R is the reorientation correlation time of the nuclei, R_{ke} is the relaxation rate of the unpaired electron, and τ_j is the correlation time for any exchange mechanism that modulates the magnetic environment of the nuclei, e.g., the electron self-exchange (ESE) of blue copper proteins. Further, ω_I and ω_S are the Larmor frequencies of the observed nuclei and the electron, respectively, γ_I is the gyromagnetic ratio of the observed nuclei, μ_0 is the magnetic permeability in vacuum, μ_B is the Bohr magneton, and g_e the electron g value.

The relaxation corresponding to the second term in eq 1, R_{1cont}, is caused by a modulation of the Fermi contact interaction and is given by[4]

$$R_{1cont} = \frac{2}{3} S(S+1)\left(\frac{A_j}{\hbar}\right)^2 \left[\frac{\tau_{e,2}}{1+\omega_S^2\tau_{e,2}^2}\right] \tag{3}$$

where $\tau_{e,2}^{-1} = R_{2e} + \tau_j^{-1}$ and $A_j/\hbar$ is the electron−nuclear hyperfine coupling constant.

The third contribution, R_{1Curie}, is the Curie spin relaxation. It is due to the modulation of the interaction between the nuclear spin and the static electron magnetic moment and has the form[5,6]

$$R_{1Curie} = \frac{2}{5}\left(\frac{\mu_0}{4\pi}\right)^2 \frac{S^2(S+1)^2 g_e^4 \mu_B^4 \gamma_I^2 B_0^2}{(3kT)^2 r_M^6}\left[\frac{3\tau_{Rj}}{1+\omega_I^2\tau_{Rj}^2}\right] \tag{4}$$

where $\tau_{Rj}^{-1} = \tau_R^{-1} + \tau_j^{-1}$, k is the Boltzman constant, T is the temperature, and B_0 is the magnetic field strength.

The Larmor frequency of the electron, ω_S, is orders of magnitude higher than the Larmor frequency of the nuclei, ω_I, i.e., 658 times that of the proton, 2600 times that of carbon, and 6600 times that of nitrogen. Furthermore, the effective correlation rates, $\tau_{c,k}^{-1}$ and $\tau_{e,2}^{-1}$, that apply to the blue copper proteins are relatively slow due to the slow electron relaxation rate of Cu(II) proteins, the slow reorientation rate of the protein molecule, and the negligible contribution from the exchange rate, τ_j^{-1}, corresponding to the electron self-exchange process in mixed samples of oxidized and reduced *A.v.* PCu. Therefore, at the magnetic field strengths applied here $\omega_S\tau_{c,2} \gg 1$ and $\omega_S\tau_{e,2} \gg 1$. Consequently, the second term in eq 2 is negligible. Also R_{1cont} is negligible for nuclei more than 3−4 Å from the copper atom, since it is several orders of magnitude smaller than R_{1dip} for any practical A_j values. Finally, the Curie-spin relaxation is insignificant here and can be neglected because of the small $\tau_R/\tau_{c,1}$ ratio of the blue copper proteins (at a field strength of 11.7 T, the Curie-spin relaxation is significant only if $\tau_R/\tau_{c,1} > 3 \times 10^3$). Accordingly, the equation for the longitudinal paramagnetic relaxation rate in the blue copper proteins reduces to

$$R_{1p} = \frac{2}{5}\left(\frac{\mu_0}{4\pi}\right)^2 S(S+1) g_e^2 \mu_B^2 \gamma_I^2 \Delta^2 \left[\frac{\tau_{c,1}}{1+\omega_I^2\tau_{c,1}^2}\right] \tag{5}$$

In the one center point−dipole approximation where $\Delta = r_M^{-3}$, as assumed in Solomon's original formalism,[1] the unpaired electron spin density is located entirely on the metal ion. For shorter electron−nuclei distances, this approximation holds for protons,[7] assuming that Fermi contact interaction can be neglected. A similar conclusion was made for carbons in a series of detailed relaxation studies of metal complexes of amino acids.[8−10] However, for longer distances and in particular in the case of heteronuclei, the one center point−dipole approximation breaks down, and dipolar interaction with unpaired electron spin density delocalized to the $2p_z$ orbitals of the ligand heteronuclei must be taken into account.[2] In these cases Δ^2 is given by[2,11]

$$\Delta^2 = r_M^{-6} + a r_L^{-6} (\rho^\pi)^2 + b r_M^{-3} r_L^{-3} \rho^\pi \tag{6}$$

assuming that the normalized unpaired spin density on the metal ion (ρ_M) is ~1. The first and the second terms in eq 6 refer, respectively, to the dipolar coupling of the nucleus with the

(3) Ma, L.; Led, J. J. *J. Am. Chem. Soc.* **2000**, *122*, 7823−7824.
(4) Solomon, I.; Blomembergen, N. *J. Chem. Phys.* **1956**, *25*, 261−266.
(5) Guéron, M. *J. Magn. Reson.* **1975**, *19*, 58−66.
(6) Vega, A. J.; Fiat, D. *Mol. Phys.* **1976**, *31*, 347−355.
(7) Bertini, I.; Donaire, A.; Luchinat, C.; Rosato, A. *Prot. Struct., Funct., Genet.* **1997**, *29*, 348−358.
(8) Led, J. J. *Mol. Phys.* **1980**, *40*, 1293−1313.
(9) Led, J. J. *J. Phys. Chem.* **1984**, *88*, 5531−5537.
(10) Led, J. J. *J. Am. Chem. Soc.* **1985**, *107*, 6755−6765.
(11) Mispelter, J.; Momenteau, M.; Lhoste, J. In *Biological Magnetic Resonance: NMR of Paramagnetic Molecules*; Berliner, L. J., Reuben, J., Eds.; Plenum Press: New York, 1993; Vol 12, pp 299−355.

metal-centered unpaired electron spin and the unpaired spin delocalized to the $2p_z$ orbital of the carbon or nitrogen atoms. The third term results from a correlation between the metal-centered and the delocalized unpaired electron spin. The parameter ρ^π is the normalized unpaired electron spin density in the $2p_z$ orbital of the heteronuclei, and r_L is the distance from the nucleus to the delocalized electron spin. In the heteronuclear relaxation case, r_L is averaged over Hartee−Fock−Slater atomic orbitals,[12] i.e., $r_L^{-3} = \langle r^{-3}\rangle_{2p}$. For carbon atoms $r_L^{-3} = 1.35 \times 10^{25}$ cm^{-3}, while for nitrogen atoms $r_L^{-3} = 2.43 \times 10^{25}$ cm^{-3}. In the proton relaxation case, r_L is the C−H bond length (1.1 Å) or the N−H bond length (1.0 Å). According to Mispelter et al.,[11] the values of a and b in eq 6 are 0.16 and −0.4, respectively, for heteronuclear relaxation, and 0.116 and 0.59 cos(2ϕ), respectively, for proton relaxation, where ϕ is the angle between metal−proton vector and the C−H or N−H bond.

The contribution to the relaxation rate from the delocalized unpaired electron spin, ρ^π, is considerable even for small values of ρ^π. Thus, for a nucleus with $r_M = 10$ Å and $\rho^\pi = 0.05\%$, the ratios of the three terms in eq 6 are 1:23.6:−4.9 for nitrogens, 1:7.3:−2.7 for carbons, 1:0.029:0.3 cos(2ϕ) for nitrogen-bound protons and 1:0.016:0.22 cos(2ϕ) for carbon-bound protons. If $r_M = 15$ Å and $\rho^\pi = 0.01\%$, the ratios are 8.8:94.4:−28.8 for nitrogens, 8.8:29.2:−16.0 for carbons, and 8.8:0.12:1.75 cos(2ϕ) for nitrogen−bound protons, while 8.8:0.065:1.31 cos(2ϕ) for carbon-bound protons. Hence, for heteronuclei the second and the third terms dominate eq 6 at longer distances; i.e., the nuclear paramagnetic relaxation rate (R_{1p}) is dominated by the interactions with the *ligand*-centered unpaired electron spin density rather the *metal*-centered. Even for protons, the relaxation caused by dipolar interaction with the unpaired electron spin density delocalized to the $2p_z$ orbitals of the adjacent heteronucleus is significant for protons more than 15 Å from the metal ion.

In the derivation of eqs 5 and 6, it is assumed that the bulk electron spin densities outside the local $2p_z$ orbital of a given heteronucleus (or in the case of protons outside the directly bound heteronucleus) is located on the metal ion; i.e., it is assumed that the point dipole approximation applies to this part of the spin density. Thus, it is not taken into account that a considerable part of the electron spin density is delocalized to the surrounding ligand atoms and, in particular, to those directly bound to the metal ion. Canters et al.[13] investigated this problem by calculating the electron−nuclei dipolar interaction for oxidized azurin, assuming that 40% of the electron spin was delocalized to the metal-bound ligand atoms. However, the resulting dipolar interaction was equal to or only slightly larger than the interaction obtained if all the electron spin was located on the Cu^{2+} ion. Even for a delocalization of 50−60% of the unpaired electron spin density to the metal-bound residues, as found for blue copper proteins,[14,15] the metal-centered point dipole approximation applies reasonably well for distances larger than 3 Å from the metal-bound nuclei.[2] Thus, for $r_M \geq 3$ Å, it seems reasonable to use the metal-centered point dipole approximation to evaluate the dipolar interaction of the nuclei with the unpaired electron spin density outside the local $2p_z$ orbitals. For $r_M \leq 3$ Å, the point dipole approximation may break down.[11] For blue copper proteins, this limit could be somewhat higher considering the larger electron delocalization to the metal-bound ligand atoms (50−60%).

The Influence of Electron Self-Exchange on Longitudinal Relaxation. In mixed samples of oxidized and reduced *A.v.* PCu, the electron self-exchange affects the NMR spectra considerably through chemical exchange, even though the modulation of the electron−nuclei interactions caused by the ESE process is too slow to influence the nuclear R_{1p} relaxation (vide supra). Thus, in a mixed system of reduced and oxidized *A.v.* PCu where electron self-exchange takes place, the nuclei will exchange between two different chemical environments. In this case, the observed resonances depend on both environments, and their time dependences are described by the McConnell equations for a two-site exchange system.[16] Hence, the longitudinal magnetization of the diamagnetic species and its time dependence is given by the complete solution of these equations:[17]

$$M_d(t) = C_1 e^{\lambda_- t} + C_2 e^{\lambda_+ t} + M_d^\infty \tag{7}$$

$$\lambda_- = -\frac{1}{2}\{(k_{1d} + k_{1p}) - [(k_{1d} - k_{1p})^2 + 4f_d f_p K^2]^{1/2}\} \tag{8}$$

$$\lambda_+ = -\frac{1}{2}\{(k_{1d} + k_{1p}) + [(k_{1d} - k_{1p})^2 + 4f_d f_p K^2]^{1/2}\} \tag{9}$$

$$C_1 = [(\lambda_+ + k_{1d})(M_d^\infty - M_d^0) - f_p K((M_p^\infty - M_p^0)]/(\lambda_- - \lambda_+) \tag{10}$$

$$C_2 = [-(\lambda_- + k_{1d})(M_d^\infty - M_d^0) + f_p K((M_p^\infty - M_p^0)]/(\lambda_- - \lambda_+) \tag{11}$$

Here K is the exchange rate which, in the case of electron self-exchange, is given by $K = k_{ese}c$, where k_{ese} is the ESE rate constant and c is the total concentration of the protein. Further, $k_{1d} = f_p K + R_{1d}$ and $k_{1p} = f_d K + R^*_{1p}$, where f_d and f_p are the molar fraction of the diamagnetic and paramagnetic species, respectively, and R_{1d} and R^*_{1p}(= $R_{1p} + R_{1d}$) are the intrinsic longitudinal relaxation rates of the nuclei in the two sites, respectively, in the absence of exchange. Finally, M_d^∞ and M_p^∞ are the equilibrium longitudinal magnetizations in the two sites, respectively, and M_d^0 and M_p^0 are the corresponding initial magnetizations immediately after the radio frequency perturbation.

As shown by eq 7, the decay of the longitudinal magnetization is, in general, biexponential. However, it becomes monoexponential in two extreme cases, i.e., the fast-exchange case that applies when $K \gg R^*_{1p} - R_{1d}$ and the slow-exchange case that applies when $K \ll R^*_{1p} - R_{1d}$. In the first case, the longitudinal magnetization in the two sites relax with a common R_1 rate:[18]

$$R_{1o} = R_{1d} + f_p R_{1p} \tag{12}$$

where R_{1o} is the relaxation rate of the observed signal(s). In the second case, the longitudinal magnetization in the two sites relax with individual R_1 rates where the relaxation rate in the diamagnetic site is given by[18]

$$R_{1o} = R_{1d} + K f_p \tag{13}$$

In the intermediate case where none of the two extreme exchange conditions apply, the magnetization is, in principle,

(12) Morton, J. R.; Preston, K. F. *J. Magn. Reson.* **1978**, *30*, 577−582.
(13) Canters, G. W.; Hill, H. A. O.; Kitchen, N. A. *J. Magn. Reson.* **1984**, *57*, 1−23.
(14) Werst, M. M.; Davoust, C. E.; Hoffman, B. M. *J. Am. Chem. Soc.* **1991**, *113*, 1533−1538.
(15) Kalverda, A. P.; Salgado, J.; Dennison, C.; Canters, G. W. *Biochemistry* **1996**, *35*, 3085−3092.
(16) McConnell, H. M. *J. Chem. Phys.* **1958**, *28*, 430−431.
(17) Led, J. J.; Gesmar, H. *J. Magn. Reson.* **1982**, *49*, 444−463.
(18) McLaughlin, A. C.; Leigh, J. S., Jr. *J. Magn. Reson.* **1973**, *9*, 296−304.

biexponential. However, if only one of the two involved relaxation rates, R_{1p}^* and R_{1d}, is very small compared to the exchange rate, the second exponential in eq 7 vanishes much faster than the first one, and the decay becomes effectively single-exponential after a certain short delay. Consequently λ_- can be obtained from a relaxation experiment with a suitable set of time delays. In the case of *A. v.* PCu, where the R_{1d} rates are much smaller than *K*, decays calculated from eq 7 are single-exponential with rates given by $-\lambda_-$ for any realistic R_{1p} value, if the delay is longer than 10 ms. Under these conditions the observed relaxation rates are given by

$$R_{1o} = -\lambda_- = \frac{R_{1d} + R_{1p}^* + K}{2} - \left[\left(\frac{R_{1p} + K}{2}\right)^2 - Kf_pR_{1p}\right]^{1/2} \quad (14)$$

From eq 14 the following expression can be derived:

$$R_{1p} = \frac{(R_{1o} - R_{1d} - K)(R_{1o} - R_{1d})}{R_{1o} - R_{1d} - Kf_p} \quad (15)$$

Using eq 15, the R_{1p} rates can be calculated from the experimental data if exchange takes place between the diamagnetic and paramagnetic sites ($K > 0$).

Since oxidized PCu is paramagnetic, the changes of the NMR parameters caused by the oxidized form can be rather dramatic. Indeed, the presence of the paramagnetic species may lead to complete obliteration of the NMR signals of nuclei close to the metal ion, if the concentration of the paramagnetic species is sufficiently high and the electron self-exchange rate is sufficiently fast.

Materials and Methods

Sample Preparation. Plastocyanin from *Anabaena variabilis* (*A.v.* PCu) was prepared and purified as described previously.[19] Aprotinin was added during the purification to minimize enzymatic degradation of *A.v.* PCu. The protein was dissolved in 99.9% D_2O except for the ^{15}N-enriched *A.v.* PCu samples and a sample used for ^{1}H NOESY experiments where it was dissolved in 90% H_2O/10% D_2O. The protein concentrations were from 2.9 to 3.2 mM in the sample of unlabeled *A.v.* PCu and from 4.1 to 4.4 mM in the ^{15}N-enriched *A.v.* PCu samples, with 100 mM NaCl added in all cases. The pH varied from 6.9 to 7.3. The oxidized *A.v.* PCu(I) was prepared by adding an equimolar amount of $K_3[Fe(CN)_6]$ to *A.v.* PCu(II). The partially oxidized samples were obtained by mixing the appropriate amounts of *A.v.* PCu(I) and *A.v.* PCu(II) or, alternatively, by adding the corresponding amount of $K_3[Fe(CN)_6]$ to *A.v.* PCu(I). Small amounts (0.6−0.7 mM) of sodium ascorbate were added to the samples of reduced *A. v.* PCu to maintain the copper in the reduced state. The protein solutions were flushed with nitrogen to remove oxygen, and the NMR tubes were sealed off under nitrogen.

NMR Experiments. The NMR experiments were carried out on Varian Unity Inova spectrometers equipped with *z*-axis pulsed-field gradient triple-resonance probes, and operating at the magnetic field strengths of 11.7 and 17.6 T, corresponding to ^{1}H frequencies of 500 and 750 MHz, respectively. All experiments were performed at 298 K. The ^{1}H carrier was placed on the HDO resonance (4.774 ppm at 298 K), while the ^{13}C and ^{15}N carriers were set at 67 and 120 ppm, respectively. All 2D spectra were acquired with hypercomplex quadrature detection in the t_1 dimension using the States−Haberkorn−Ruben method.[20] In the 2D heteronuclear experiments, ^{13}C and ^{15}N decoupling was performed during acquisition using the WALTZ-16 scheme.[21]

One-dimensional inversion recovery experiments were used to measure the longitudinal ^{1}H relaxation rates at 500 and 750 MHz. Each experiment consisted of 11−19 spectra with delay times ranging from 0.008 to 9.0 s. A recovery delay of 9 s was applied between scans, and 32 scans were recorded for each spectrum. The relaxation delays were chosen randomly to compensate for possible systematic drift.

The R_1 relaxation rates of the methine carbons of *A.v.* PCu were obtained at 125 and 188 MHz from samples with ^{13}C in natural abundance using the 2D heteronuclear ^{1}H−^{13}C pulse sequence.[22,23] A 5-ms purge pulse followed by a 0.5-ms *z*-gradient pulse were applied to suppress the solvent signal and the resonances from ^{12}C-bound protons. The protons were saturated during the ^{13}C recovery delay by a series of 90° pulses separated by 7 ms, to ensure a single-exponential decay of the carbon magnetization.[1] The time domain signals consisted of 128 t_1 slices each with 2048 data points. For the series recorded at 125 MHz, the sweep width was 6025 in the ^{1}H dimension and 4400 Hz in the ^{13}C dimension. For the series recorded at 188 MHz, the corresponding sweep widths were 9000 and 6600 Hz, respectively. A recovery delay of 2.5 s was applied between scans, and 256 scans were recorded for each slice.

The ^{13}C R_1 experiments consisted of nine 2D spectra with delay times of 0.01, 0.1, 0.2, 0.4, 0.8, 1.2, 1.8, 2.5, and 4.5 s, respectively. The entire acquisition time was 13.5 days. To eliminate errors caused by systematic drift of the spectrometers and by minor changes in the degree of oxidation of the partly oxidized samples, each one of the nine 2D spectra was effectively recorded over the entire acquisition period; i.e., each t_1 slice in all nine 2D spectra was averaged over the 13.5-day acquisition period. This was achieved by recording all 9 × 128 t_1 slices in a recurrent manner over 8 cycles with 32 scans in each cycle; i.e., in each cycle, 32 scans were recorded of the *n*th slice (n = 1−128) in the *k*th spectrum, *k* being varied from 1 to 9 for each value of *n*. The same procedure was applied in the R_1 series recorded at ^{13}C 188 MHz where seven 2D spectra with delay times of 0.01, 0.1, 0.2, 0.4, 0.8, 1.2, and 2.5 s were acquired in 7 days.

The ^{15}N R_1 rates were obtained at 50.7 MHz from 95% ^{15}N enriched *A.v.* PCu samples using the ^{1}H−^{15}N pulse sequence by Farrow et al.[24] The pulsed field gradients applied in this sequence allowed a minimization of artifacts, suppression of the intense solvent resonance, and selection for the coherence transfer pathway that allows indirect observation of ^{15}N through ^{1}H. The time domain signals consisted of 320 t_1 slices each with 2048 data points. The sweep width was 10 000 Hz in the ^{1}H dimension and 2000 Hz in the ^{15}N dimension. A recovery delay of 1.5 s was applied between scans, and 32 scans were recorded for each slice. Eleven 2D spectra were recorded in each R_1 experiment, with delay times of 0.010, 0.020, 0.040, 0.080, 0.160, 0.321, 0.501, 0.702, 0.903, 1.203, and 1.905 s, respectively. The entire acquisition time was 19.5 h for each experiment. The 2D spectra in each R_1 experiment were recorded simultaneously using the same recurrent procedure as applied in the ^{13}C R_1 experiments.

The ^{1}H NOESY spectra were recorded as described previously,[19] except that the water resonance was suppressed by a WATERGATE scheme.[25] Mixing times of 60 and 120 ms were used both in H_2O and D_2O solutions. The sweep width was 10 000 Hz in both dimensions. The $^3J_{\alpha\beta}$ coupling constants were obtained from an E-COSY spectrum[26] of reduced *A.v.* PCu in D_2O recorded on a Bruker AM 500 spectrometer.

(19) Badsberg, U.; Jørgensen A. M. M.; Gesmar, H.; Led, J. J.; Hammerstad, J. M.; Jespersen, L. L.; Ulstrup, J. *Biochemistry* **1996**, *35*, 7021−7031.

(20) States, D. J.; Haberkorn, R. A.; Ruben, D. J. *J. Magn. Reson.* **1982**, *48*, 286−292.

(21) Shaka, A. J.; Keeler, J.; Frenkiel, T.; Freeman, R. *J. Magn. Reson.* **1983**, *52*, 335−338.

(22) Palmer, A. G., III; Rance, M.; Wright P. E. *J. Am. Chem. Soc.* **1991**, *113*, 4371−4380.

(23) Mispelter, J.; Lefévre, C.; Adjadj, E.; Quiniou, E.; Favaudon, V. *J. Biomol. NMR* **1995**, *5*, 233−244.

(24) Farrow, N. A.; Muhandiram, R.; Singer, A. U.; Pascal, S. M.; Kay, C. M.; Gish, G.; Shoelson, S. E.; Pawson, T.; Forman-Kay, J. D.; Kay, L. E. *Biochemistry* **1994**, *33*, 5984−6003.

(25) Piotto, M.; Saudek, V.; Sklenar, V. *J. Biomol. NMR* **1992**, *2*, 661−665.

(26) Griesinger, C.; Sørensen, O. W.; Ernst, R. R. *J. Magn. Reson.* **1987**, *75*, 474−492.

The 2D spectra obtained in the ^{13}C and ^{15}N R_1 experiments were processed using NMRPipe[27] running on a DEC Ultra Workstation 533au. The ^{13}C FIDs were zero-filled to 4096 and 512 data points and the ^{15}N FIDs to 4096 and 1024 data points in the t_2 and t_1 dimensions, respectively. An exponential line-broadening of 5 Hz was applied in the t_2 dimension, while a sine-bell window function was applied in the t_1 dimension. No baseline correction was used. The processing of the 1D spectra and 2D NOESY and E-COSY spectra was performed on a DEC3000 AXP 400 workstation using in-house written software. No window function or zero-filling were applied for the 1D R_1 data set. In the 2D NOESY spectra, an exponential line-broadening of 15 Hz was used in both dimensions while a zero-filling was applied that results in a resolution of 4.9 and 9.8 Hz point^{-1} in t_2 and t_1 dimensions, respectively. The window functions used for the E-COSY spectrum were a 45° phase shifted sine bell, a 90° phase shifted squared sine bell, and a line-broadening of 5 Hz in both dimensions.

Structure Determination. Interproton distance restraints were obtained from the NOESY experiments detailed above. The volumes of the signals were determined by a combination of linear prediction analysis and least-squares estimation.[28,29] The NOEs were classified as weak, medium, or strong with corresponding upper limits of 5.0, 3.56, and 2.85 Å as described previously,[19] except for the intraresidual NOEs used to characterize a preferred rotamer conformation. For these NOEs, the upper limits were 4.0, 3.4, and 3.1 Å for weak, medium, and strong NOEs, respectively.[30]

The structures were calculated with the program X-PLOR 3.851 using distance geometry, simulated annealing, and restrained energy minimization.[31] The paramagnetic relaxations of the ^{13}C and ^{15}N nuclei in the metal-bound ligand residues revealed unambiguously that the copper atom is bound to the same donor atoms as in other plastocyanins, that is, δN of His39, δN of His92, γS of Cys89, and δS of Met97.[19] The copper atom was included in the distance geometry simulated annealing (DGSA) and refine calculations with the geometric constraints reported by Moore et al.[32] included in the applied parameter file, i.e., parallhdg.pro (X-PLOR). These constraints are the bonds between Cu−δN His39 (2.05 Å), Cu−δN His 92 (2.05 Å), Cu−γS Cys89 (2.12 Å), and Cu−δS Met97 (2.90 Å). A force constant of 70 kcal mol^{-1} Å^{-2} was used for all four bonds. Further, the following angles were used: X−Cu−X angles (X = S or N) of 110° and a force constant of 10 kcal mol^{-1}rad^{-2}, Cu−N−C angles of 127° and a force constant of 50 kcal mol^{-1}rad^{-2}, and Cu−S−C angles of 120° and a force constant of 50 kcal mol^{-1}rad^{-2}. The force constant on the X−Cu−X angles was chosen to allow ±28° distortions from the tetrahedral geometry.[32] The van der Waals radii of the copper atom was set to 2.2 Å. Finally, the χ_1 angles were restrained to 60°, 180° or −60° ± 60° for the g^2g^3, g^2t^3 and t^2g^3 conformations, respectively.

The protocols used in the structure calculation were essentially those proposed in the X-PLOR manual (dg_sub_embed.inp, dgsa.inp and refine.inp).[31] A total of 60 substructures were calculated and run through 200 cycles of restrained energy minimization and 6-ps restrained molecular verlet dynamics at 3000 K followed by a 10-ps cooling to 100 K and 200 cycles of restrained energy minimization. In the refine protocol, the structures were heated to 3000 K and then slowly (20 ps) cooled to 100 K. The time steps were 0.003 and 0.005 ps for the high-temperature dynamics and the cooling step, respectively. Finally, the structures were run through 200 cycles of restrained energy minimization. The van der Waals function was represented by a simple repel function in all calculations. The 20 structures with the lowest total energy were selected for further analysis.

Estimation of the R_1 Relaxation Rates. The intensities of the signals in the R_1 experiments were determined by a least-squares fitting procedure[29] whereby all intensities of a given resonance in a series of relaxation spectra were determined simultaneously. Since the frequency, line width, and phase of each resonance remain unchanged through the series, this procedure reduces the number of parameters drastically and, thus, increases the precision by which the R_1 rates can be obtained.

In the experiments used to determine the ^{15}N R_1 rates, the signals decay toward zero, and the intensities were, therefore, analyzed by a least-squares fit using the two-parameter exponential function:

$$M(t) = M^0 \exp(-R_1 t) \tag{16}$$

In the experiments used to determine the ^{13}C and ^{1}H R_1 relaxation rates, the signals decay toward a maximum steady-state value. Accordingly the intensities were analyzed by a least-squares fit using the three-parameter exponential function:

$$M(t) = M^\infty + (M^0 - M^\infty) \exp(-R_1 t) \tag{17}$$

In eqs 16 and 17, M^0 is the initial value of the magnetization immediately after inversion pulse, M^∞ is the steady-state value of the magnetization, and $M(t)$ is the value of the magnetization at time t.

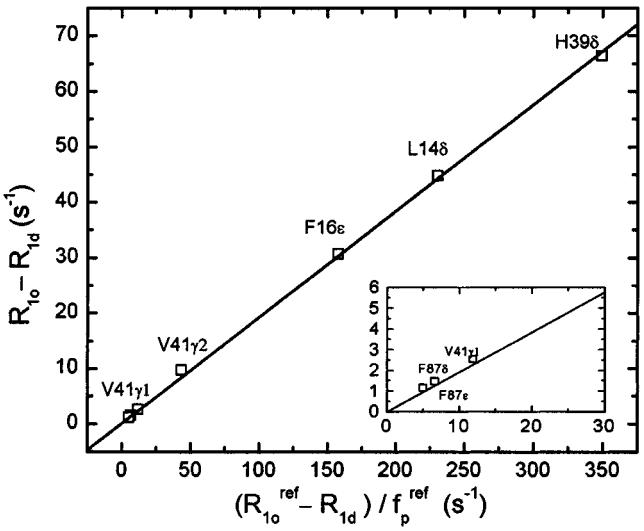

Figure 1. Estimation of the fraction, f_p, of oxidized *A.v.* PCu from a plot of the relaxation enhancements, $R_{1o} - R_{1d}$, of selected protons versus the corresponding normalized relaxation enhancements of a reference sample, using eq 12. The inset is an expansion of the left part of the plot. The linear curve corresponds to a fit of eq 12 to the experimental data; f_p is given by the slope of the curve. For the sample corresponding to the actual plot $f_p = 19.1 \pm 0.6\%$. The R_{1o}^{ref} rates were obtained from a reference sample with 5% oxidized *A.v.* PCu (i.e., $f_p^{ref} = 0.05$).

Estimation of the Fraction of Oxidized *A.v.* PCu. The fraction, f_p, of oxidized *A.v.* PCu in the samples was monitored throughout the study by measuring the R_1 rates of selected protons in the protein. When the fast-exchange condition applies, i.e., $K \gg R_{1p}$, the fraction f_p can be obtained from the R_{1o} and R_{1d} rates (eq 12) using the R_{1o} rates of a sample with a known fraction of oxidized *A.v.* PCu as a reference. For a given electron self-exchange rate, K, the fast-exchange condition applies to nuclei that have a sufficiently slow R_{1p} rate, i.e., nuclei that are sufficiently far away from the metal ion. Figure 1 shows plots of $(R_{1o} - R_{1d})$ versus $(R_{1o}^{ref} - R_{1d}^{ref})/f_p^{ref}$ for a series of resonances that fulfill the fast-exchange condition. The linearity of the plot in Figure 1 confirms that this condition applies to the selected protons. The use of this method to estimate f_p was essential in the present study, since the oxidation degree of the samples varied slightly over time. Therefore, f_p was estimated before and after each experiment, and the average f_p value was used in the data analysis. This procedure, in combination with the recurrent manner in which all 2D experiments were recorded (vide supra), ensured a reliable estimation of the effective f_p values and, thus, of the R_{1p} rates.

(27) Delagio, F.; Grzesiek, S.; Vuister, G. W.; Zhu, G.; Pfeifer, J.; Bax, A. *J. Biomol. NMR* **1995**, *6*, 277−293.
(28) Gesmar, H.; Nielsen, P. F.; Led, J. J. *J. Magn. Reson.* **1994**, *B103*, 10−18.
(29) Kristensen, S. M.; Sørensen, M. D.; Gesmar, H.; Led, J. J. *J. Magn. Reson.* **1996**, *B112*, 193−196.
(30) Basus, V. J. *Methods Enzymol.* **1989**, *177*, 132−149.
(31) Brünger, A. T. *X-PLOR version 3.1. A system for crystallography and NMR*; Yale University: New Haven, CT, 1992.
(32) Moore, J. M.; Lepre, C. A.; Gippert, G. P.; Chazin, W. J.; Case, D. A.; Wright, P. E. *J. Mol. Biol.* **1991**, *221*, 533−555.

Table 1. Structural Statistics for *A.v.* Plastocyanin

Number of Constraints	
total number of NOEs	1459
intraresidue NOEs	595
sequential NOEs	279
interresidue NOEs	585
ϕ angle	49
χ^1 angle	29
ω angle	9
rms Deviations from NOE Restraints and from the Idealized Geometry Used within X-PLOR[a]	
NOE (Å)	0.017 ± 0.003
bond length (Å)	0.0031 ± 0.0008
bond angles (deg)	1.06 ± 0.02
improper dihedral angles (deg)	0.42 ± 0.02
PROCHECK Ramachandran Analysis[a]	
most favored regions (%)	59.2
additional allowed regions (%)	36.4
generously allowed regions (%)	3.4
disallowed regions (%)	0.9
Average rms Deviations from the Mean Structure[a]	
all heavy atoms[b] (Å)	1.21
backbone atoms[b] (Å)	0.75
all β-sheet heavy atoms[c] (Å)	0.90
β-sheet backbone atoms[c] (Å)	0.52

[a] Fitting was done on the final ensemble of 20 refined structures with the lowest total energy. [b] Rms deviations for all heavy atoms and for all N, C_α, and C′ backbone atoms, respectively, of Thr2-Ala104. [c] Rms deviations for all heavy atoms and for all N, C_α, and C′ backbone atoms from the β-sheet region, respectively. The β-sheet region included the residues from Thr2 to Leu7, Leu14 to Pro18, Lys20 to Lys24, Asp27 to Asn33, Pro37 to Asp44, Gln70 to Phe76, Gly83 to Cys89, and Met97 to Ala104.

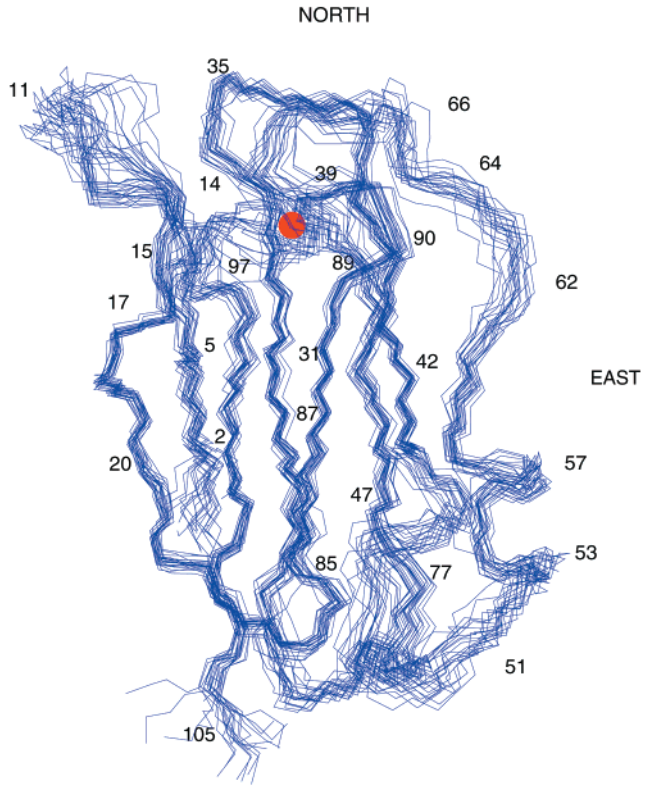

Figure 2. Best-fit superposition of the 20 refined solution structures of *A.v.* PCu with the lowest total energy. Only the C′, C_α, and N backbone atoms for the β-sheet region are superimposed. This region included Thr2−Leu7, Leu14−Pro18, Lys20−Lys24, Asp27−Asn33, Pro37−Asp44, Glu70−Pro76, Gly83−Cys89, and Met97−Ala104.

Results and Discussion

Refined Structure. The NMR solution structure of *A.v.* PCu determined previously[19] was refined by including stereospecific assignments of a series of β-protons and the methyl groups of most of the valines and leucines in the structure calculation. The total number of NOEs was 1459, including 595 intraresidual, 279 sequential, and 585 interresidual NOEs. Furthermore, 49 ϕ angles obtained from the $^3J_{H_\alpha H_N}$ coupling constant, 9 proline ω angles, and 29 χ^1 angles were included. The structural statistics are given in Table 1.

The conformations of the χ^1 angles and the stereospecific assignment of the H_β protons were derived from the $^3J_{\alpha\beta}$ coupling constant and the intraresidual $d_{\alpha\beta}$ and $d_{\beta N}$ NOEs.[30,33] The $^3J_{\alpha\beta}$ coupling constants were obtained from the passive coupling in an E-COSY spectrum, defining $^3J_{\alpha\beta} > 11$ Hz as a large coupling constant and $^3J_{\alpha\beta} < 5$ Hz as a small coupling constant. Observation of only one of the intraresidual α,β signals in both the E-COSY and the DQF-COSY spectrum was taken as an indication of a large coupling constant if supported by a weak α,β NOE, and a small coupling constant if supported by a strong α,β NOE. Using these criteria, 7 g^2g^3, 5 g^2t^3, and 15 t^2g^3 rotamers were assigned stereospecifically, of the total number of 57 β-CH_2 groups in *A.v.* PCu. Another three β-CH_2 groups were assigned as either g^2t^3 or t^2g^3 by excluding the g^2g^3 conformation on the basis of the $^3J_{\alpha\beta}$ coupling constants. The 29 χ^1 angles mentioned above were restrained according to these assignments and were included in the structure calculation together with 27 pairs of stereospecifically assigned β-CH_2 protons.

The stereospecific assignment of the γ-methyl groups of valine was based on the $^3J_{\alpha\beta}$ coupling constant and the intraresidual $d_{\alpha\gamma}$ and $d_{\gamma N}$ proton NOEs using the same procedure.[30] Immediately five CH_3 groups of valine, i.e., Val5, Val36, Val41, Val42, and Val103, could be identified as g^+ rotamers due to the large $^3J_{\alpha\beta}$ coupling constants. Subsequently the stereospecific assignment of the γ-methyl groups could be deduced from the intraresidual $d_{\gamma N}$ NOEs, except for Val36 where the stereospecific assignment was obtained from the calculated structures and NOEs to spatially adjacent protons. The remaining three valines, Val15, Val29, and Val98, have only small $^3J_{\alpha\beta}$ coupling constants and are, therefore, either t or g^- rotamers. The methyl group of Val15 could be identified as t according to the observed $d_{\alpha\gamma}$ and $d_{\gamma N}$ NOEs. For Val29, the stereospecific assignment was obtained from the structure, while for Val98, no stereospecific assignment of the methyl groups could be made.

For eight of the nine prolines, stereospecific assignment of the β-protons was made on the basis of the $d_{\alpha\beta}$ NOEs by exploiting the fact that the β^2-proton is always closer to the α-proton than the β^3-proton.[34] For Pro49, stereospecific assignment was not possible due to signal overlap of one of the α,β NOEs. The side-chain amide protons of two Asn residues and one Gln residue were stereospecifically assigned using the NOEs between the NH atoms and the adjacent methylene group.[34] Finally, the stereospecific assignment of the δ-CH_3 groups of 6 of the 10 Leu residues was obtained from the calculated structure and NOEs to spatially adjacent protons.

A best-fit superposition of the backbone of the 20 structures with the lowest total energy is shown in Figure 2. No NOE violation larger than 0.2 Å and no dihedral angle violation larger

(33) Wagner, G.; Braun, W.; Havel, T. F.; Schaumann, T.; Go, N.; Wüthrich, K. *J. Mol. Biol.* **1987**, *196*, 611−639.

(34) Kline, A. D.; Braun, W.; Wüthrich, K. *J. Mol. Biol.* **1988**, *204*, 675−724.

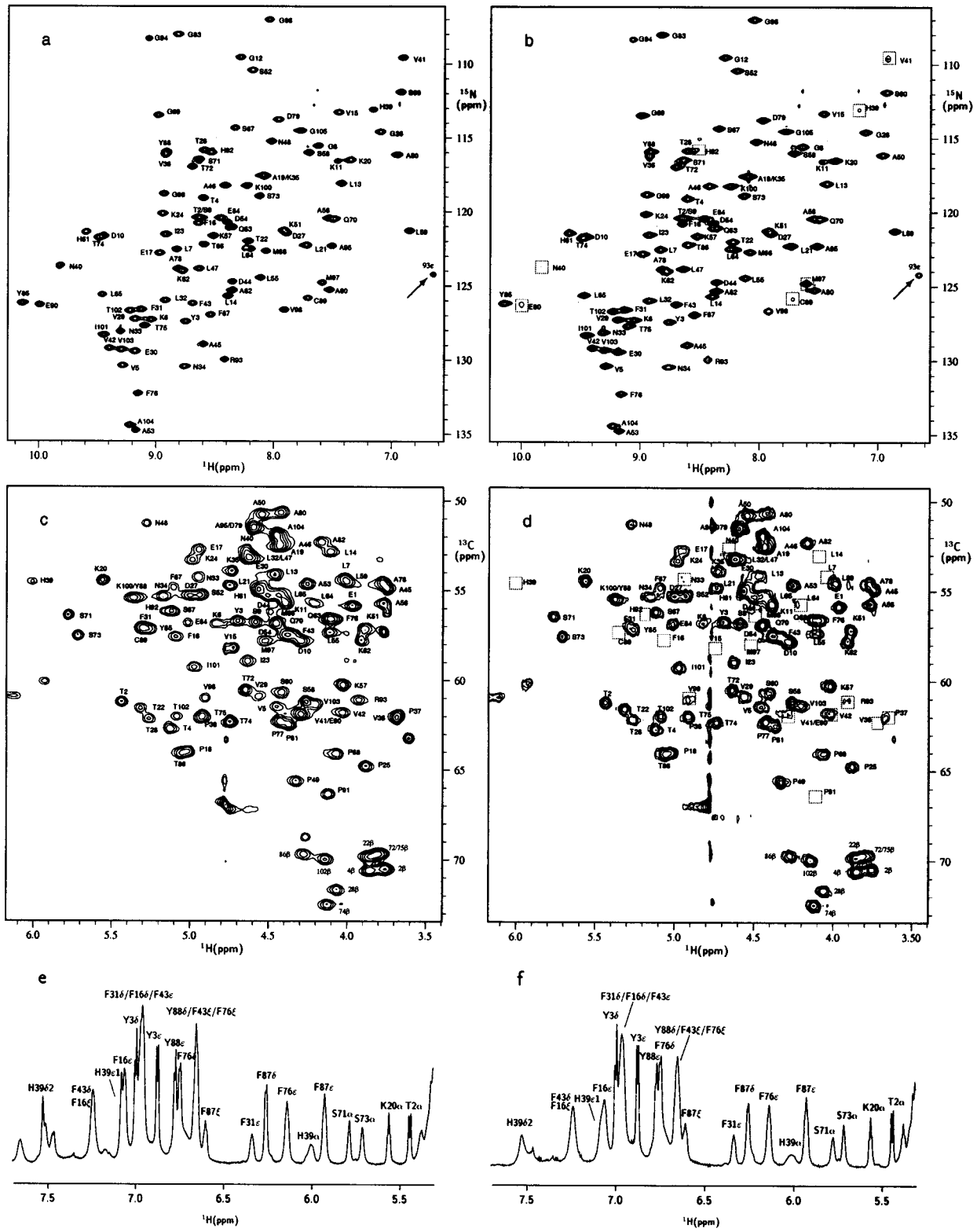

Figure 3. Panels a−d: fingerprint regions of the 2D R_1 spectra of *A.v.* PCu at 11.7 T corresponding to the shortest delay time; (a) and (b) are the ^{1}H−^{15}N correlation spectra of reduced and 9% oxidized *A.v.* PCu, respectively; the arrows indicate the folded signal from Arg93N$^\epsilon$; (c) and (d) are the ^{1}H−^{13}C correlation spectra of reduced and 18% oxidized *A.v.* PCu, respectively. The boxes in (b) an (d) indicate signals for which the intensities are appreciably reduced in the partly oxidized *A.v.* PCu. Panels e and f: ^{1}H inversion recovery spectra of *A.v.* PCu at 750 MHz corresponding to the longest delay time; (e), reduced *A.v.* PCu; (f), 15.5% oxidized *A.v.* PCu.

than 5° were observed in the 20 structures. The general fold of the structure is identical to that found in the previous study.[19] However, the structure obtained here is significantly better defined, in particular the helical region from Ala53 to Ser60 which is a regular α helix in the refined structure.

Assignment of NMR Spectra of Partially Oxidized *A.v.* PCu. The spectra of reduced and oxidized *A.v.* PCu (Figure 3) show identical patterns with only slightly fewer signals in the spectra of the oxidized form, even at relatively high PCu(II) concentrations. This holds despite the general assumption that

Cu(II) proteins are less suitable for NMR studies due to severe line-broadening and reflects the fact that the electron relaxation in *A.v.* PCu(II) is relatively fast[3] and dominates the effective correlation rate (vide infra). Still considerable line-broadening is observed for a number of signals in the oxidized samples, in particular in the ^{13}C relaxation spectra, resulting in severe signal overlap (Figure 3c and d).

The chemical shifts of the resonances in the partially oxidized samples used here are only slightly different from those observed in the reduced sample. Thus, in the 10% oxidized sample, the changes in chemical shifts relative to those of reduced *A.v.* PCu varied only from -3 to $+7$ Hz for the nitrogens, from -5 to $+7$ Hz for the carbons, and from -10 to $+10$ Hz for the protons. Further, the shifts could easily be followed in the spectra with increasing f_p values. Therefore, the spectra of the partially oxidized samples were assigned unambiguously on the basis of previous assignment of the proton spectrum[19] of reduced *A.v.* PCu and the corresponding ^{13}C and ^{15}N spectra (to be published).

In copper proteins, the Fermi contact shifts, ω_{FC}, of the nuclei in the ligand residues are considerable, whereas pseudocontact shifts, ω_{PC}, caused by the dipole−dipole interaction between the nuclei and the unpaired electron of the Cu(II) ion, are small if the protein has a type-I copper center,[15] as in plastocyanins. Therefore, the small shifts observed here show that the "well-resolved" condition[18] ($\omega_{FC} \gg K$) applies to the ligand residues resulting in different signals for reduced and oxidized *A.v.* PCu, while the "exchange-narrowing" condition[18] ($\omega_{PC} \ll K$) applies to the more remote residues where the Fermi contact shift is negligible, resulting in average signals for the two forms.

The R_1 Rates in Reduced and Partially Oxidized *A.v.* PCu. The R_{1d} and R_{1o} rates were measured for a series of nuclei in *A.v.* PCu, including the ^{15}N and $^{13}C_\alpha$ nuclei, and a series of side-chain ^{13}C nuclei and protons. The R_{1o} rates of ^{15}N were obtained from five partly oxidized samples with PCu(II) ranging from 9 to 36%, while the corresponding ^{13}C and ^{1}H rates were obtained from a sample with 18% PCu(II). The ^{15}N rates were measured at 11.7 T while the ^{13}C and ^{1}H rates were measured at both 11.7 and 17.6 T. To ensure determination of the largest possible number of relaxation rates with the highest possible precision, the rates were extracted by a simultaneous least-squares analysis of all spectra in a relaxation experiment, as described under Materials and Methods. Single-exponential decays were assumed in all cases, as discussed in the Theoretical Section. Two-parameter fits (eq 16) were used to obtain the ^{15}N rates while three-parameter fits (eq 17) were used to extract the ^{13}C and ^{1}H R_1 rates. Typical R_1 decay curves are shown in Figure 4. The obtained ^{15}N, ^{13}C, and ^{1}H relaxation rates are given in Supporting Information.

The R_{1d} relaxation rates were obtained for 91 of the 95 backbone nitrogens, excluding the nitrogens of the N-terminal and the 9 proline, while the R_{1o} rates were obtained for 87 backbone nitrogens. The R_1 rates of two side-chain nitrogens, His39N$^\epsilon$ and Arg93N$^\epsilon$, located outside the applied sweep width were obtained from the folded signals (see Figure 3a and b). The uncertainties of the intensities were typically $\leq$1%, while the uncertainties of the ^{15}N R_1 rates in the reduced and the 9% oxidized plastocyanin sample were $\leq$0.5% for most of the signals and $\leq$3% for all signals. The uncertainties of the R_{1o} rates obtained from the other oxidized samples are in the range from 0.3 to 2%.

The obtained ^{13}C rates are less precise due to the applied natural abundance of the ^{13}C nuclei, the relatively low protein concentration, and the severe signal overlap. Still, the simultaneous data-fitting procedure allowed an estimation of 82 C_α relaxation rates from the reduced sample and 75 C_α rates from the oxidized sample. In addition, the R_1 rates of 18 of the 29 side-chain methine carbons were determined for reduced plastocyanin while 13 rates were obtained for the partly oxidized form. The uncertainties of the intensities were typically $\leq$3−20% and the uncertainties of the R_1 rates $\leq$10%.

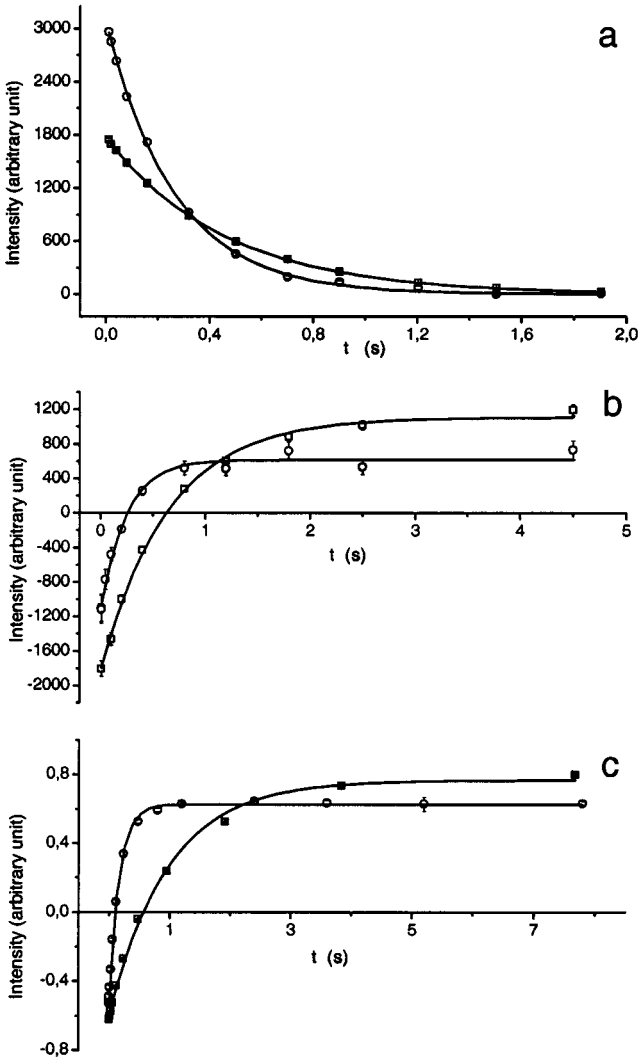

Figure 4. Examples of decay curves corresponding to the relaxation of nuclei in *A.v.* PCu; (a) His39 backbone ^{15}N in reduced (□, $R_{1d} = 2.162 \pm 0.008$ s^{-1}) and 9% oxidized (○, $R_{1o} = 3.76 \pm 0.07$ s^{-1}) *A.v.* PCu; (b) Leu7 $^{13}C_\alpha$ in reduced (□, $R_{1d} = 1.586 \pm 0.081$ s^{-1}) and 18.0% oxidized (○, $R_{1o} = 3.61 \pm 0.39$ s^{-1}) *A.v.* PCu; (c) Val41 $H_{\gamma 2}$ in reduced (□, $R_{1d} = 1.045 \pm 0.061$ s^{-1}) and 15.5% oxidized (○, $R_{1o} = 5.87 \pm 0.12$ s^{-1}) *A.v.* PCu.

The proton R_1 rates were determined for 21 well-resolved ^{1}H resonances in the aliphatic and aromatic regions of the 1D inversion−recovery spectra. The aromatic region is shown in Figure 3e and f. The R_{1d} and R_{1o} rates of four α-protons, eight methyl protons, and nine aromatic protons were obtained for both reduced and 18% oxidized plastocyanin. The uncertainties of the intensities were typically $\leq$4% and the uncertainties of the estimated R_1 rates $\leq$8%.

Paramagnetic Longitudinal Relaxation of Nuclei in *A.v.* PCu. The experimental data including their uncertainties, i.e., the R_{1d} and R_{1o} rates, and the fractions, f_p, of oxidized plastocyanin, allow a reliable estimation of the R_{1p} rates using eq 15 and a k_{ese} rate constant[35] at 298 K of 3.2×10^5 M^{-1} s^{-1}. Variation of k_{ese} in the range from 2.0×10^5 to 4.0×10^5 M^{-1}

s^{-1} has only negligible influence on the calculated R_{1p} rates of the ^{15}N and ^{13}C nuclei and most of the protons. Only the values calculated for the R_{1p} rates of the fast-relaxing protons of the ligand-bound H39 residue depend significantly on the K value. This dependence, however, allows a lower limit of the k_{ese} rate constant to be estimated from the experimental relaxation rates of the fastest relaxing proton, i.e., H39 H^{α}. For this proton, the slow-exchange condition ($K \ll R^{*}_{1p} - R_{1d}$) and eq 13 are nearly fulfilled because of its fast R_{1p} rate ($\sim$1500 s^{-1}, Table S7 in supporting Information). Accordingly, using eq 3, the rates $R_{1o} = 108\ s^{-1}$ and $R_{1d} = 0.63\ s^{-1}$ obtained for H39 H^{α} at $f_p = 0.18$ and $c = 2.9$ mM (Table S7) give a k_{ese} rate constant of $2.0 \times 10^5\ M^{-1}\ s^{-1}$, i.e., a value that is only slightly smaller than the value applied here.

The R_{1p} rates were estimated for all the 89 observed ^{15}N nuclei at 11.7 T. The average rates obtained from the five partially oxidized samples are shown in Figure 5a. The R_{1p} values range from 0.05 to 125 s^{-1} with uncertainties typically from 5 to 20%. Further, the R_{1p} rates of 41 α-carbons and seven side-chain methine carbons were estimated at both 11.7 and 17.6 T, with rates ranging from 0.4 to 34 s^{-1} at 11.7 T (Figure 5b) and from 0.4 to 185 s^{-1} at 17.6 T (data not shown) with uncertainties typically from 25 to 100%. The remaining ^{13}C nuclei, for which the R_1 rates were determined, have negligible paramagnetic relaxation enhancement. Finally, the R_{1p} of the 21 protons investigated here are in the range from 0.2 to 1513 s^{-1} at 11.7 T (Figure 5c) and from 0.3 to 838 s^{-1} at 17.6 T (data not shown) with uncertainties from 10 to 110%.

It should be emphasized, that the above estimation of the R_{1p} rates requires use of the correct, individual R_{1d} rates in eq 15, rather than a common average value.[7] Thus, for example, at 500 MHz the proton R_{1d} rates obtained here vary considerably, ranging from about 0.5−0.6 s^{-1} for aromatic protons, over 0.6−0.7 s^{-1} for the α-protons, to almost 2 s^{-1} for some of the side-chain protons (see Supporting Information). In particular, it is essential to use the proper R_{1d} rates for nuclei that are more than 8−10 Å from the metal ion where the R_{1d} rates are larger than the paramagnetic relaxation enhancement.

Differences between the structures or the dynamics of reduced and oxidized plastocyanin could result in different R_{1d} rates in the two forms. This could introduce errors in the estimated R_{1p} rates since the R_{1d} rates of the reduced form were used in the calculation of the R_{1p} rates from eq 15. As for the structures of the two forms, an overall agreement is indicated by the identical patterns in the spectra of reduced and oxidized *A.v.* PCu (Figure 3). The structural similarity is also indicated by the correlation shown in Figure 5, between the R_{1p} rates of the oxidized form and the corresponding distances in the solution structure of the reduced form. Furthermore, observation of the same NOEs in the $^1H-^1H$ NOESY spectra of the reduced and partially oxidized samples indicates similar secondary and tertiary structures. In support of this agreement, it was found that the rmsd of the backbone in reduced and oxidized plastocyanin from the fern *Dryopteris crassirhizoma*[37] is only 0.16 Å in the crystal structures and that the structure of the metal site region remains unchanged upon oxidation. A similar agreement was found for the backbones in the crystal structure of reduced and oxidized poplar plastocyanin,[38] although in this case a dissociation of His87 from the copper atom was observed for the reduced form.

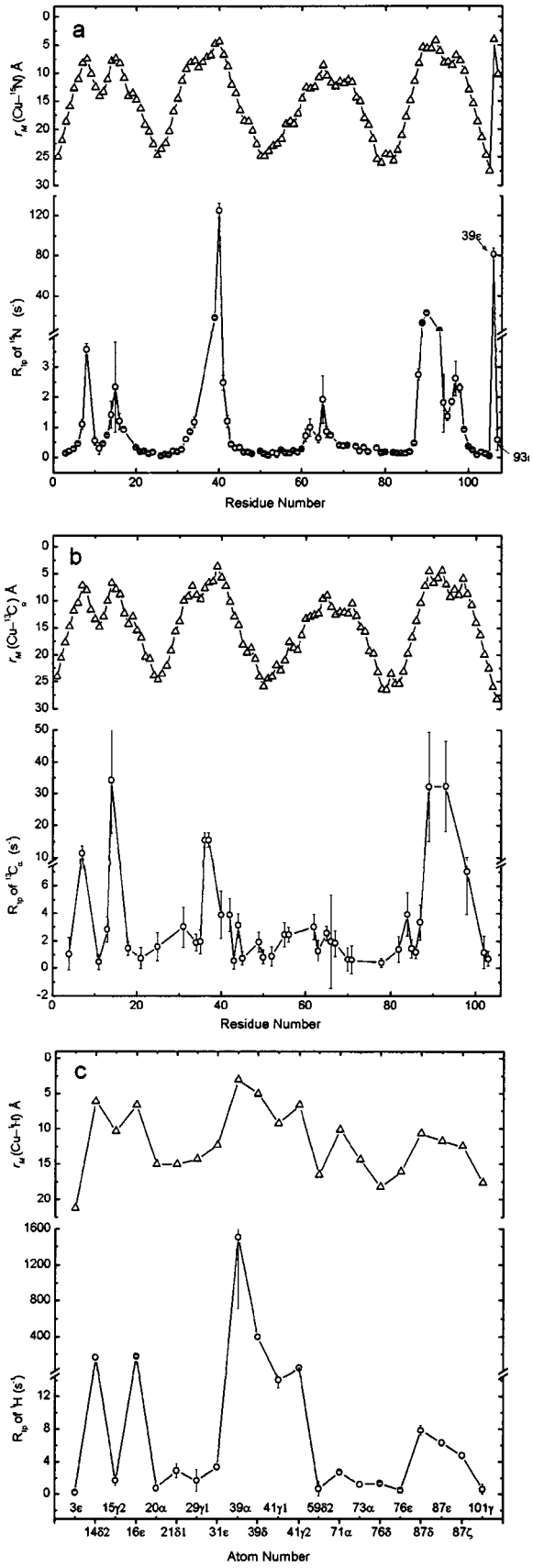

Figure 5. Lower curves: Variation with sequence position of R_{1p} rates of nuclei in *A.v.* PCu at 11.7 T; (a) 87 backbone ^{15}N and two side-chain ^{15}N; (b) 41 $^{13}C_{\alpha}$; (c) 21 selected ^1H. Upper curves: The corresponding Cu−nuclei distances in the refined structure (average of the 20 structures in Figure 2). For protons in CH_2 and CH_3 groups, average Cu−^1H distances were used.

(35) Dennison, C.; Kyritsis, P.; McFarlane, W.; Sykes, A. G. *J. Chem. Soc., Dalton Trans.* **1993**, 1959−1963.
(36) Rasmussen, N. Master Thesis, University of Copenhagen, 1996.
(37) Inoue, T.; Gotowda, M.; Sugawara, H.; Kohzuma, T.; Yoshizaki, F.; Sugimura, Y.; Kai, Y. *Biochemistry* **1999**, *38*, 13853−13861.
(38) Guss, J. M.; Harrowell, P. R.; Murata, M.; Norris, V. A.; Freeman, H. C. *J. Mol. Biol.* **1986**, *192*, 361−387.

Concerning the dynamics of poplar and fern *D. crassirhizoma*, plastocyanin changes were observed in the H-bond network upon oxidation,[37,38] suggesting different flexibilities of the two forms. For heme-containing cytochromes, an increased flexibility of the oxidized form was indicated by the ^{15}N relaxation rates[39] and by increased amide hydrogen exchange rates observed upon oxidation.[40−42] Such changes in flexibility of the proteins could result in a change in the R_{1d} rates. However, even if the relaxation enhancement of 0.05−0.1 s^{-1}, which is observed in oxidized *A.v.* PCu for ^{15}N nuclei about 20−25 Å from the copper ion, reflects an increase in the R_{1d} rates caused by a higher flexibility of the oxidized form rather than a paramagnetic effect, it would only cause minor errors. Thus, for nitrogens closer than 10 Å to the copper atom, the error in the R_{1p} rates is negligible while it is 10% for ^{15}N ∼10 Å from the copper ion and 60% for nitrogens ∼19 Å from the copper ion. Errors of this size would not significantly affect the $\Delta^{-1/3}$ values discussed below.

Deviation from the Point−Dipole Approximation. A detailed analysis of the estimated R_{1p} rates can now be made on the basis of the refined NMR solution structure (Figure 2) using eqs 5 and 6. The analysis requires a precise knowledge of the effective correlation rate $\tau_{c,1}^{-1} = \tau_R^{-1} + R_{1e} + K$. Recently it was found[3] that the longitudinal electron relaxation rate R_{1e} in *A.v.* PCu is (5.8 ± 0.5) × 10^9 s^{-1} at 11.7 T and 298 K, while a value of 1.6 × 10^8 s^{-1} was obtained[36] for τ_R^{-1} at 298 K (τ_R = 6.2 ns) in good agreement with the size of *A.v.* PCu (M_r 10.5 kDa). In comparison, the ESE rate K is only 1 × 10^3 s^{-1} at the applied *A.v.* PCu concentration[35] (vide supra). Consequently $\tau_{c,1}^{-1}$ is dominated entirely by R_{1e}.

In the point-dipole approximation, Δ in eq 2 is given by the distance r_M between the Cu^{2+} ion and the nuclei in the protein; that is, $\Delta = r_M^{-3}$. To test the validity here of this approximation, $\Delta^{-1/3}$ was calculated from the obtained R_{1p} rates at 11.7 T using eq 5 and the effective $\tau_{c,1}^{-1}$ correlation rate and compared with the r_M distances of the refined structures (Figure 6). The corresponding data obtained for ^{13}C and ^{1}H at 17.6 T (see Supporting Information) are in good agreement with those shown in Figure 6b and c. As it appears from Figure 6a and b, $\Delta^{-1/3} < r_M$ for all ^{15}N and ^{13}C distances. The substantial and systematic deviations clearly demonstrate that the point−dipole approximation does not apply to these nuclei. For ^{13}C, the use of natural abundance results in a relatively higher uncertainty of the data. Still, the deviation is clear and similar to that observed for ^{15}N. For ^{1}H, the deviation is less pronounced and significant only for r_M > 10 Å. A similar deviation was reported for protons in [4Fe-4S] proteins[43] where the slope of ln R_{1p}^{-1} versus ln r_M was 5.5 rather than 6 as expected from eq 2 for $\Delta = r_M^{-3}$.

The plots in Figure 6 reveal that the deviation increases with increasing r_M values and almost isotropically within the protein. The latter is further illustrated in Figure 7 which shows the $\Delta^{-1/3}$ and r_M values of the backbone ^{15}N of the individual residues. These observations exclude that the deviation is caused by an association whereby the nuclei in a diamagnetic molecule is affected by the electron of the Cu^{2+} ion in a paramagnetic

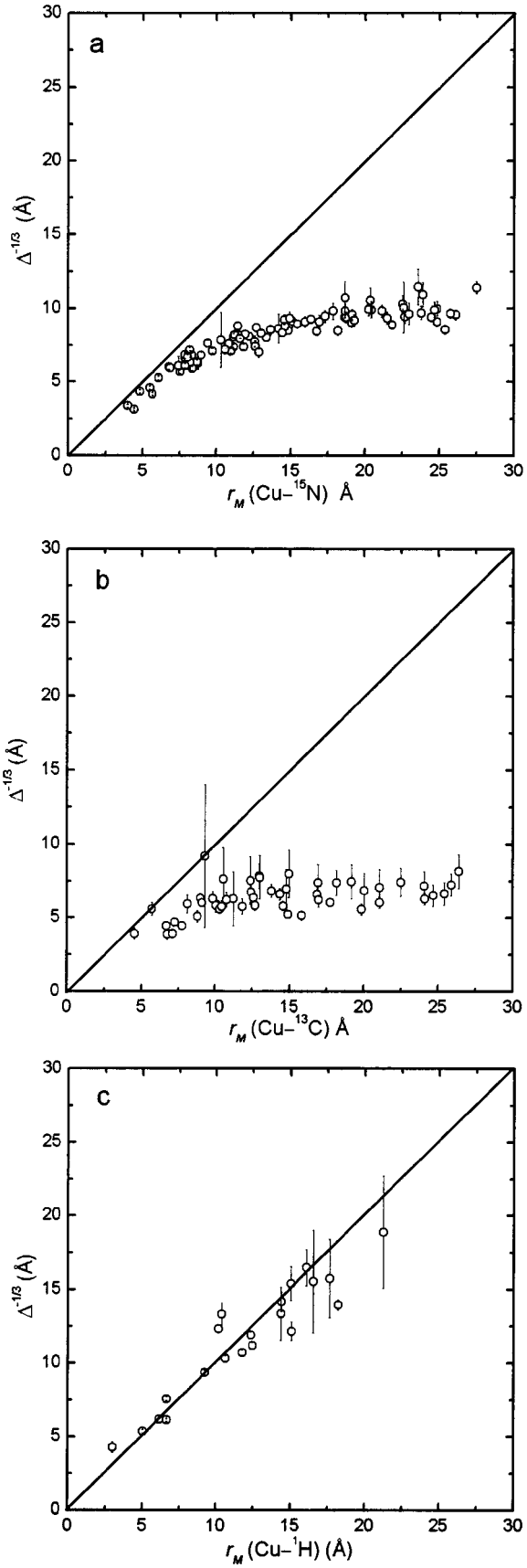

Figure 6. Comparison of the $\Delta^{-1/3}$ values of nuclei in *A.v.* PCu (calculated from the R_{1p} rates at 11.7 T, using eq 5) and the corresponding Cu−nuclei distances, r_M, in the refined structure (average of the 20 structures in Figure 2); (a) 87 backbone ^{15}N and two side-chain ^{15}N; (b) 41 $^{13}C_\alpha$ and seven side-chain methine ^{13}C; (c) 21 selected ^{1}H.

(39) Fetrow, J. S.; Baxter, S. M. *Biochemistry* **1999**, *38*, 3380−4492.
(40) Arnesano, F.; Banci, L.; Bertini, I.; Felli, I. C. *Biochemistry* **1998**, *37*, 173−184.
(41) Banci, L.; Bertini, I.; Bren, K. L.; Gray, H. B.; Sompornpisut, P.; Turano, P.; Felli, I. C. *Biochemistry* **1997**, *36*, 8992−9001.
(42) Banci, L.; Bertini, I.; Gray, H. B.; Luchinat, C.; Reddig, T.; Rosato, A.; Turano, P. *Biochemistry* **1997**, *36*, 9867−9877.
(43) Huber, J. G.; Moulis, J.; Gaillard, J. *Biochemistry* **1996**, *35*, 12705−12711.

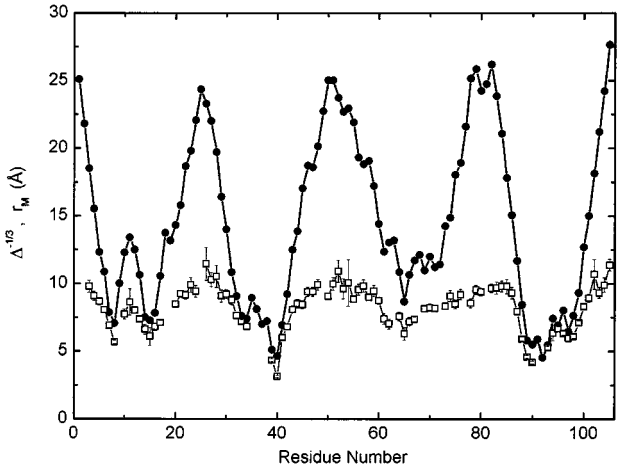

Figure 7. Variation with sequence position of the $\Delta^{-1/3}$ values (□) for 87 backbone ^{15}N nuclei in *A.v.* PCu calculated from the R_{1p} rates at 11.7 T using eq 5 and the corresponding Cu−^{15}N distances, r_M, (●) in the refined structure (average of the 20 structures in Figure 2).

molecule. Although such associations would primarily affect the remote nuclei close to the surface of the protein, as observed here, the effect would be more pronounced in regions with high docking probability. Furthermore, among the nuclei of the surface residues, the hydrogens are closer to the surface and interact more strongly with the electron because of a larger gyromagnetic ratio than the ^{15}N and ^{13}C nuclei. Therefore, an association would result in a larger effect on ^{1}H than on ^{15}N and ^{13}C in sharp contrast to the observations.

Also, spin diffusion can be ruled out as a source of the deviation. In the case of the heteronuclei, spin diffusion is effectively eliminated by the ^{1}H decoupling during the evolution period (t_1) of the experiment (vide supra). Furthermore, for protons, theoretical calculations[7] using CORMA[44] indicate that spin diffusion can cause only a small increase (<20%) of the paramagnetic relaxation enhancement of ^{1}H and, therefore, cannot account for the discrepancy between $\Delta^{-1/3}$ and r_M observed here for the remote protons (Figure 6c). Finally, an increase in mobility of the observed nuclei on the picosecond time scale could in principle result in increased $\Delta^{-1/3}$ values since the extreme narrowing condition ($\omega_I^2\tau_{c,1}^2 \leq 1$) applies to the heteronuclei at the magnetic field strengths used here.[3] In practice, however, any reasonable increase of $\tau_{c,1}^{-1}$, in particular for backbone heteronuclei, has only negligible effect on R_{1p} and $\Delta^{-1/3}$ as discussed above.

The deviation from the point−dipole approximation that is clearly demonstrated by the systematic discrepancy between $\Delta^{-1/3}$ and r_M in Figure 6 is, therefore, caused entirely by the delocalization of the unpaired spin of Cu^{2+} ion onto the $2p_z$ orbital of the carbon and nitrogen atoms. Indeed, such delocalization is in qualitative agreement both with the uniform distribution of the deviation throughout the molecule and with the substantially smaller effect observed for the protons that are affected only by the electron delocalization onto the $2p_z$ orbitals of the adjacent heteronuclei. Hence, the experimental results obtained here show that the relaxation of the ^{15}N and ^{13}C nuclei is dominated by dipolar interaction with the delocalized unpaired spin density given by the second and third terms in eq 6, while dipolar interaction with the metal-centered unpaired electron spin given by the first term has only little significance. Consequently, the R_{1p} rates of the ^{15}N and ^{13}C nuclei do not provide information about the nuclear−metal ion distances in any straightforward way. In contrast, the smaller deviation observed for ^{1}H suggests that distance information can be obtained from the R_{1p} rates for protons up until ~10 Å from the metal ion, despite the delocalization of the unpaired electron spin density to the $2p_z$ orbitals of adjacent heteronuclei.

Spin Delocalization and Relation to Long-Range Electron Transfer. The unpaired electron spin densities ρ^π delocalized to the $2p_z$ atomic orbital of the ^{15}N and ^{13}C nuclei of the protein were calculated from the R_{1p} rates and the r_M distances in the refined average *A.v.* PCu structure (Figure 2) using eqs 5 and 6. The ρ^π densities obtained range from 0.007 to 0.372% for ^{15}N and from 0.02 to 0.19% for ^{13}C (Figure 8). As it appears from the two lower plots in Figure 8, the ρ^π values decrease approximately exponentially with increasing r_M distances. A least-squares analysis shows that the decays correspond broadly (see however below) to the equation

$$\rho^\pi = 0.00011 + 0.003e^{-0.3(r_M - 0.5)} \qquad (18)$$

where r_M is in Å. Only ρ^π values of nuclei more than 6 Å from the copper atom were included in the fitting to omit possible electron delocalization caused by Fermi contact interactions with the copper-bound ligand residues (see the Theoretical Section).

The delocalization of the unpaired electron spin of the metal ion onto the local ^{15}N- or ^{13}C-based $2p_z$ orbitals of the ligand residues and the more remote protein structure is carried both by "direct" delocalization of excess unpaired electron *density* and by spin *polarization*.[45] The latter refers to correlation between the unpaired electron spin at the metal center and $2p_z$-localized spins of *paired* electrons at the heteronuclei. Spin densities extracted from the dipolar coupling between the local nuclear spins and the delocalized unpaired electron spin densities (Figure 8) incorporate both effects.

Electron density and spin polarization decay differently along the bond system. Electronic density delocalization through the protein has been mapped in some detail in long-range electron transfer (ET).[46] In some cases, a single delocalization or ET route dominates, as reflected in more or less approximately exponential decay of the ET rate along this route.[47] In other cases, several routes contribute,[48] reflected in more or less isotropic exponential decays with the geometric donor−acceptor distance. This accords roughly with a view of tunneling through energetically and spatially averaged barriers in the structurally anisotropic environment.

As shown above, the data in Figure 8 can be recast in approximately exponential form, but the simple view of exponential electron density delocalization from ET does not straightaway carry over to unpaired spin delocalization. Exponential electron density delocalization takes the approximate form[46]

$$\psi_D \approx \psi_D^0 + \frac{\beta_D}{\Delta E_D}\exp\left[-\frac{1}{a}\left(\ln\frac{\Delta}{\beta}\right)R\right]\psi_{B_N}^0 \qquad (19)$$

where ψ_D^0 is the donor wave function and $\psi_{B_j}^0$ ($j = 1, ..., N$) are wave functions for electron localization on the intermediate groups. The constant β_D couples the donor with the first intermediate group, β is the average coupling between nearest-

(44) Keepers, J. W.; James, T. L. *J. Magn. Reson.* **1984**, *57*, 404−426.

(45) La Mar, G. N. In *NMR of Paramagnetic Molecules. Principles and Applications*; La Mar, G. N., Horrocks, W. De W., Jr., Holm, R. H., Eds.; Academic Press: New York, 1973; p 85.

(46) Kuznetsov, A. M.; Ulstrup, J. *Electron Transfer in Chemistry and Biology. An Introduction to the Theory*; Wiley: Chichester, 1999.

(47) Winkler, J. R.; Gray, H. B. *Chem. Rev.* **1992**, *92*, 369−379.

(48) Moser, C. C.; Page, C. C.; Chen, X.; Dutton, P. L. *J. Biol. Inorg. Chem.* **1997**, *2*, 393−398.

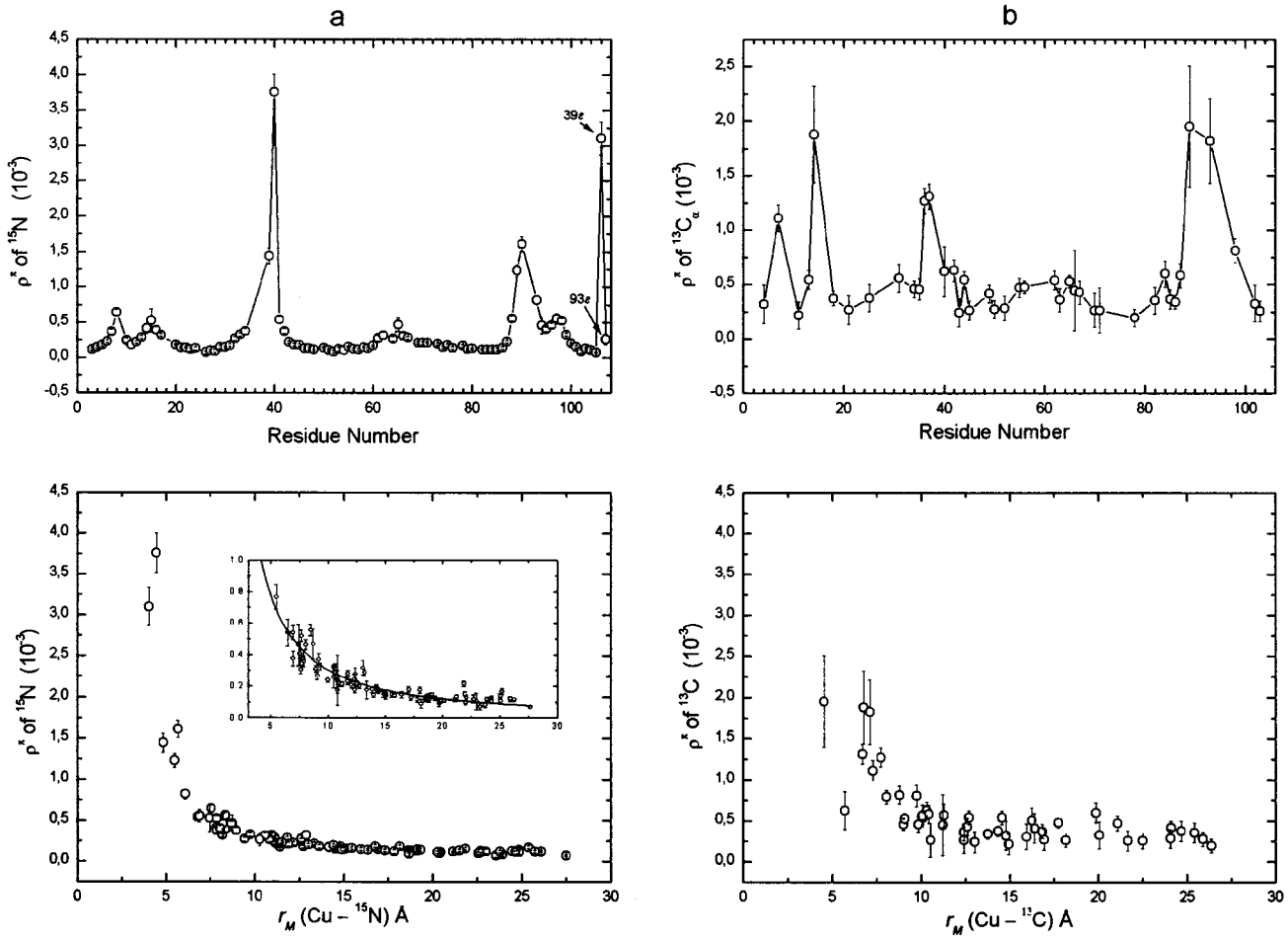

Figure 8. Spin densities ρ^{π} in the local $2p_z$ orbitals of heteronuclei in *A.v.* PCu; (a) 87 backbone ^{15}N and two side-chain ^{15}N; (b) 41 $^{13}C_{\alpha}$ and seven side-chain methine ^{13}C. Upper plots: Variation of ρ^{π} with sequence position. Lower plots: Variation of ρ^{π} with Cu−nuclei distance in the refined structure of *A.v.* PCu (average of the 20 structures in Figure 2). The fitted curve in the lower plot of the ^{15}N data (inset) is given by $\rho^{\pi} = 0.00011 + 0.003e^{-0.3(r_M - 0.5)}$. The fit only includes ρ^{π} values of nuclei more than 6 Å from the copper atom to omit possible electron delocalization caused by Fermi contact interactions with copper-bound ligand residues.

neighbor intermediate groups, while Δ is the average energy gap between the donor and the intermediate group. Finally, R is the distance along a particular route and a the intermediate group extension. Electron localization is thus stronger, the larger the energy gap and the smaller the couplings.

Many experimental protein ET data accord with an exponential form, with decay factors of $\sim$1−1.4 Å^{-1}.[47,48] Decay factors for intramolecular ET in synthetic molecular systems are mostly smaller, i.e., 0.5−0.8 Å^{-1}.[46] In comparison the spin delocalization in Figure 8 extends further, with a decay factor of $\sim$0.3 Å^{-1}. This suggests that the spin density pattern cannot be caused solely by electron density delocalization but must be assisted by spin polarization.

In comparison with "direct" electron delocalization, spin polarization is an "indirect" effect.[45,49,50] The unpaired electron density remains at the metal ion but induces spin redistribution in paired orbitals along the peptide backbone. Spin polarization is thus caused by different correlations between the metal unpaired electron and the two spins of the paired electrons in ^{15}N- and ^{13}C-based $2p_z$ orbitals. This has the following implications: (a) *Two* parallel delocalization mechanisms invoke weaker spin attenuation than only a single mechanism. (b) The data in Figure 8 represent combined delocalization of electron *density* and unpaired *spin*. This is not in conflict with intramolecular ET data as these rest solely on electron density decay. (c) Spin density decay and electron density decay are different phenomena but follow the same routes through the protein. In turn, this holds implications for long-range ET. Thus, (d) spatial mapping of the *spin* density is unique by directly monitoring experimentally the density along different specific routes. In comparison, detection of intermediate group contributions in *electron* transfer is always indirect and rests on the distance dependence of the rate constant. Further, (e) *spin* delocalization clearly follows routes in different directions. This extends to *electron* transfer which is, however, also controlled by the protein surface structure. The combination of tunneling routes and surface molecular recognition thus determines the sites for actual ET.[46,51] Finally, (f) an intriguing observation is that the spin delocalization onto ^{15}N and ^{13}C of Cys89, Met66, Met97, and other nearby ^{15}N and ^{13}C nuclei is notably higher than for other residues at comparable distances from the copper atom and thus falls outside the broadly exponential decay given by eq 18. This accords with sulfur-containing residues as particularly efficient electron transmitters, due to their ligand function (Cys89, Met97),[52] or high electronic polarizability.[48] The new

(49) (a) Orgel, L. E. *Discussions Faraday Soc.* **1958**, *26*, 92−93. (b) Orgel, L. E. *J. Chem. Phys.* **1959**, *30*, 1617−1618.
(50) Levy, D. A.; Orgel, L. E. *Mol. Phys.* **1961**, *3*, 583−587.
(51) Christensen, H. E. M.; Conrad, L. S.; Mikkelsen, K. V.; Nielsen, M. K.; Ulstrup, J. *Inorg. Chem.* **1990**, *29*, 2808−2816.
(52) Solomon, E. I.; LaCroix, L. B.; Randall, D. W. *Pure Appl. Chem.* **1998**, *70*, 799−808.

observation in the present work provides the first experimental substantiation of such views.

Conclusions

The detailed analysis of the longitudinal paramagnetic relaxation of ^{15}N and ^{13}C in *A.v.* PCu shows, in conjunction with the obtained refined NMR solution structure of the protein, that the relaxation is dominated by dipolar interaction with unpaired electron spin density delocalized onto the local $2p_z$ orbitals of the nuclei. In consequence of this, the point−dipolar approximation does not apply to these nuclei, and their distances from the metal ion can, therefore, not be obtained from the R_{1p} rates in any straightforward way. For protons, the R_{1p} rates seem less affected by the delocalization of the unpaired electron spin density, suggesting that ^{1}H-metal distances shorter than ∼10 Å can be estimated from these rates.

The detailed analysis of the R_{1p} rates in combination with the refined structure of the protein also allows a quantitative determination of the unpaired electron spin densities, ρ^π, that is delocalized onto the individual heteronuclei. This determination reveals an almost isotropic, exponential decay of ρ^π with increasing distance from the metal ion with clear implications for the long-range ET patterns of the protein. However, the decay is slower than normally found for ET reactions, suggesting that an extra mechanism contributes to the spin delocalization in parallel with the electron density delocalization of ET, namely, spin polarization of the paired electrons in the ^{15}N- and ^{13}C-based $2p_z$ orbitals induced by the metal-centered unpaired electron.

Acknowledgment. We thank Dr. Søren M. Kristensen for providing the program used to estimate the signal intensities and for helpful discussions, Prof. N. G. Carr and Dr. J. Scanlan, University of Warwick, for the donation of several *A.v.* samples, Mrs. Lise-Lotte Jespersen for purifying the plastocyanin, and Mrs. Else Philipp for technical assistance with the 500-MHz spectrometer and the sample preparations. The 750-MHz spectra were obtained at The Danish Instrument Center for NMR Spectroscopy of Biological Macromolecules. The study was financially supported by the Danish Natural Science Research Council (J. 9400351, 9502759 and 9801801), the Danish Technical Research Council (3.9801629), Julie Damm's Studiefond, Direktør Ib Henriksens Fond, Novo Nordisk Fonden and Carlsbergfondet.

Supporting Information Available: Tables of R_1 rates and spin densities: the experimental R_{1d}, R_{1o}, and R_{1p} rates in *A. v.* plastocyanin of ^{13}C and ^{1}H at 11.7 and 17.6 T and of ^{15}N at 11.7 T, together with the corresponding calculated paramagnetic relaxation rates (R_{1p}) and delocalized electron spin densities (ρ^π) (PDF). Tables of constraints: χ^1, ω, and ϕ angle constraints and NOE-derived distance constraints used in the structure calculation of *A. v.* plastocyanin (PDF). This material is available free of charge via Internet at http//pubs.acs.org. The NMR-derived restraints have been deposited in the RCSB (Research Collaboratory for Structural Bioinformatics) Protein Data Bank together with coordinates of the 20 refined structures with lowest energy (PDB accession code 1FA4).

JA001368Z